THE JOURNAL OF BIOLOGICAL CHEMISTRY VOL. 285, NO. 47, pp. 37102–37110, November 19, 2010
Printed in the U.S.A.

Polymorphic C-terminal β-Sheet Interactions Determine the Formation of Fibril or Amyloid β-derived Diffusible Ligand-like Globulomer for the Alzheimer Aβ42 Dodecamer*[S]

Received for publication, April 13, 2010, and in revised form, August 27, 2010 Published, JBC Papers in Press, September 16, 2010, DOI 10.1074/jbc.M110.133488

Buyong Ma[‡1] **and Ruth Nussinov**[‡§]

From the [‡]*Basic Science Program, SAIC-Frederick, Inc., Center for Cancer Research Nanobiology Program, National Cancer Institute, Frederick, Maryland 21702 and the* [§]*Sackler Institute of Molecular Medicine, Department of Human Genetics and Molecular Medicine, Sackler School of Medicine, Tel Aviv University, Tel Aviv 69978, Israel*

The relationship between amyloid deposition and cellular toxicity is still controversial. In addition to fibril-forming oligomers, other soluble Aβ forms (amyloid β-derived diffusible ligands (ADDLs)) were also suggested to form and to present different morphologies and mechanisms of toxicity. One ADDL type, the "globulomer," apparently forms independently of the fibril aggregation pathway. Even though many studies argue that such soluble Aβ oligomers are off fibril formation pathways, they may nonetheless share some structural similarity with protofibrils. NMR data of globulomer intermediates, "preglobulomers," suggested parallel in-register C-terminal β-sheets, with different N-terminal conformations. Based on experimental data, we computationally investigate four classes of Aβ dodecamers: fibril, fibril oligomer, prefibril/preglobulomer cluster, and globulomer models. Our simulations of the solvent protection of double-layered fibril and globulomer models reproduce experimental observations. Using a single layer Aβ fibril oligomer β-sheet model, we found that the C-terminal β-sheet in the fibril oligomer is mostly curved, preventing it from quickly forming a fibril and leading to its breaking into shorter pieces. The simulations also indicate that β-sheets packed orthogonally could be the most stable species for Aβ dodecamers. The major difference between fibril-forming oligomers and ADDL-like oligomers (globulomers) could be the exposure of Met-35 patches. Although the Met-35 patches are necessarily exposed in fibril-forming oligomers to allow their maturation into fibrils, the Met-35 patches in the globulomer are covered by other residues in the orthogonally packed Aβ peptides. Our results call attention to the possible existence of certain "critical intermediates" that can lead to both seeds and other soluble ADDL-like oligomers.

Amyloid aggregates can be related to neurodegenerative diseases, including diabetes type II (1), Alzheimer disease (AD)[2] (2), and prion ("mad cow") disease. Amyloid β (Aβ) peptide oligomerization is believed to be a major mechanism leading to neuronal cell death (3). Although increasing evidence indicates that soluble oligomers of amyloidogenic proteins are responsible for amyloidosis (4, 5) and that they are the toxic agent (6–8), the question of the mechanism through which amyloids lead to cytotoxity is still a major challenge (9–13). Similar to folding, nucleation and kinetics depend on the sequence, peptide length, and environmental conditions, such as temperature (14), concentration, pH (15), metal ions (16), and whether aggregation takes place on a surface and, if so, its properties. Together, these lead to one of the most difficult questions related to aggregate polymorphism (17): the aggregates are likely to have different preferred architectures depending on such physical factors. The problem is to figure out the polymorphic range, preferred aggregate states, pathways leading to these states, time scales, and their mechanisms of toxicity. According to the energy landscape theory, all conformations and self-assembly states pre-exist (18, 19); conditions only lead to shifts in their relative populations. Consequently, figuring these factors out is of crucial importance for understanding the disease etiology and the pharmaceutical strategy.

Experiments indicate that polymorphic Aβ oligomers can differ in their toxicity mechanisms. Although the data increasingly suggest that small oligomers play critical roles in ion channel formation (20), the relationship between amyloid deposition and cellular toxicity and the similarity to bacterial pore-forming toxins (21) are still unclear. Moreover, a range of soluble Aβ forms has also been observed. Among these, the amyloid β-derived diffusible ligands (ADDLs) were proposed to have different morphologies and to exert their toxicity through different mechanisms (22). ADDL aggregates were proposed to be highly ordered, to bind to a subset of postsynaptic proteins, and to impair synaptic plasticity and associated memory dysfunction during the early stages of AD. In addition, another form of globular amyloid β-peptide (23) was observed in the brains of patients with AD and in $A\beta_{1-42}$-overproducing transgenic mice, with the water-soluble 60-kDa "globulomer" form reported to have 12 Aβ peptides and to apparently form inde-

* This work was supported, in whole or in part, by the National Cancer Institute, National Institutes of Health under contract number HHSN261200800001E and by the Intramural Research Program of the National Institutes of Health, NCI, Center for Cancer Research.

[S] The on-line version of this article (available at http://www.jbc.org) contains supplemental Table S1 and Figs. S1–S3.

[1] To whom correspondence should be addressed: Bldg. 469, Rm. 151, NCI-Frederick, Frederick, MD 21702. Fax: 301-846-5598; E-mail: mabuyong@mail.nih.gov.

[2] The abbreviations used are: AD, Alzheimer disease; Aβ, amyloid β; ADDL, amyloid β-derived diffusible ligand; FO, fibrillar oligomer; RMSD, root mean square deviation; MD, molecular dynamics; D/H, deuterium/hydrogen.

pendently of the fibril aggregation pathway (24). Although similar to ADDLs, it also relates to early AD; unlike ADDLs, it binds specifically to dendritic processes of neurons but not glia in hippocampal cell cultures. A yet additional soluble form, Aβ*56, which is smaller than the 60-kDa globulomer, causes memory deficiency in middle-aged mice (25). Finally, "amylospheroids," which are larger soluble oligomers (26, 27) with higher mass (more than 100 kDa), were reported to have sizes of ~10–15 nm. These spherical Aβ assemblies were detected in AD and Lewy body brains.

This polymorphic range raises the questions of the major pathways through which they form, the conditions favoring each, and the presence of certain intermediate states that could be targeted. Although studies argue that soluble Aβ oligomers such as ADDLs are off fibril formation pathways, the pathways and the extent of the different structural characteristics leading to the fibrillar and ADDL states are still unclear. The lattice of soluble fibrillar oligomers differs from that of the fibril, even though fibrillar oligomers eventually mature into fibrils (28). Nonetheless, soluble oligomers and fibrils could share some structural similarity with protofibrils, for example, all may have parallel β-sheet structure (29). An NMR study of the intermediates of globulomer formation, the so-called preglobulomer, pointed to parallel in-register β-sheets in the C-terminal region, even though the N-terminal region presented different conformations (30).

In this study, we computationally investigate the structure, energy, and solvent interaction of four classes of Aβ dodecamers, including fibril, fibril oligomer, prefibril/preglobulomer cluster, and globulomer models. With the goal of understanding why fibril oligomers do not seed fibril formation directly (28), we compared the fibril and fibril oligomers. We found that the C-terminal β-sheet in the fibril oligomer is mostly curved, impeding its fast conversion to, or the seeding of, a fibril that has a highly complementary C-terminal β-sheet conformation. Based on this observation, we constructed structural models with different interaction patterns in the C-terminal β-sheet that differ in the hydrophobic Met-35 patches. We found that the major difference between fibril-forming oligomers and ADDL-like oligomers (globulomers) is in the exposure of these patches. Although the patch is necessarily exposed in fibril-forming oligomers to allow their maturation into fibril, in globulomers it appears shielded by other Aβ peptide residues.

EXPERIMENTAL PROCEDURES

Model Construction—We have simulated the double-layered fibril structure of Aβ42 with an organization similar to that of Aβ17–42, which was previously characterized based on NMR (3, 31) and molecular dynamics (MD) simulations (32–34). Based on the two possible turn types in the fibril structures of the Aβ amyloid, two initial structures were constructed by adding the N-terminal region in a parallel β-sheet organization, continuing the main region of Aβ17–42 (F1; Fig. 1*A*) or Aβ10–42 (F2; Fig. 1*B*). Essentially, the F1 model has the turn structure as in the experiment-based coordinates (hydrogen exchange data, EM, and mutational data (3); Protein Data Bank code 2BEG), whereas the F2 model has the turn proposed by us (33) and experimentally by solid state NMR (31, 35). Wu *et al.* (28) have observed that the height of Aβ42 fibrillar oligomers (FO) is only approximately half of the Aβ fibril and suggested that the FO is a single layer unit of the Aβ fibril. Consistent with this notion, we simulated the Aβ42 dodecamer with the 12 Aβ42 monomers extended in an ideal one-layer organization, with two independent runs starting from conformations taken from simulations carried out with different minimization and heating times (FO1 and FO2; Figs. 2 and 3). Prefibril/preglobulomer clusters and globulomer models are constructed from experimentally observed secondary structures and other structural information. The details are presented under "Results."

Molecular Dynamics Simulations—The peptide oligomer was solvated with a TIP3P water box with a margin of at least 10 Å from any edge of the water box. Sodium ions were added to make the overall system neutral. MD simulations were performed using the NAMD package (36) and the CHARMM 27 force field (37), with constant pressure ensembles at 1 atm and temperature at 330 K. The time step was 2 fs with a SHAKE constraint on all bonds with hydrogen atoms. Productive MD runs were performed after 5,000 steps of minimizations and three 150-ps heating and equilibration runs. The long range electrostatic interactions were calculated with the Particle-Mesh-Ewald method (38). Hydrogen bonds, root mean square deviation (RMSD), and solvent interactions are calculated using the Corman module in the CHARMM 35 program. A hydrogen bond is defined by the atom pair of a backbone carbonyl oxygen atom and an amide hydrogen atom, with a distance of less than 3.0 Å. The RMSDs are calculated with respect to the averaged structure from the 60-ns trajectory. We also calculated the average number of water molecules in contact with the backbone amide hydrogen atom (NH solvation factor), which reflect the protection factor corresponding to the D/H exchange ratio observed in experiments. Thus we calculate the backbone amide solvation for each residue, averaged over the total 60-ns simulations. The distance distributions were also averaged over the 60-ns trajectories. The calculated NH solvation factor is expected to correspond to the lower D/H exchange protection factor.

Energy Landscape and Monte Carlo Simulations—Monte Carlo simulations were used to estimate the population probabilities based on conformations obtained in the last four nanoseconds of the MD simulations. Using the CHARMM 27 force field (37) and Generalized Born with the molecular volume (39) implemented in the CHARMM package, each conformer was first minimized 1,000 cycles, and then the conformational energy was evaluated by the grid-based Generalized Born with the molecular volume. The minimization does not change the conformations obtained from the MD simulations and only relaxes the local geometries because of the thermal fluctuations that occur in the simulations. In the Generalized Born with the molecular volume calculation, no distance cutoff was used, the dielectric constant of water was set to 80, and the Debye-Huckel ionic term was 0.2 to reflect the salt effect. A total of 4,400 conformations (400 for each of the 11 oligomer models examined) were used to evaluate population probabilities. Starting from a randomly selected conformation i, another conformation $i + 1$ was randomly selected from any of the 11 models by a Monte Carlo algo-

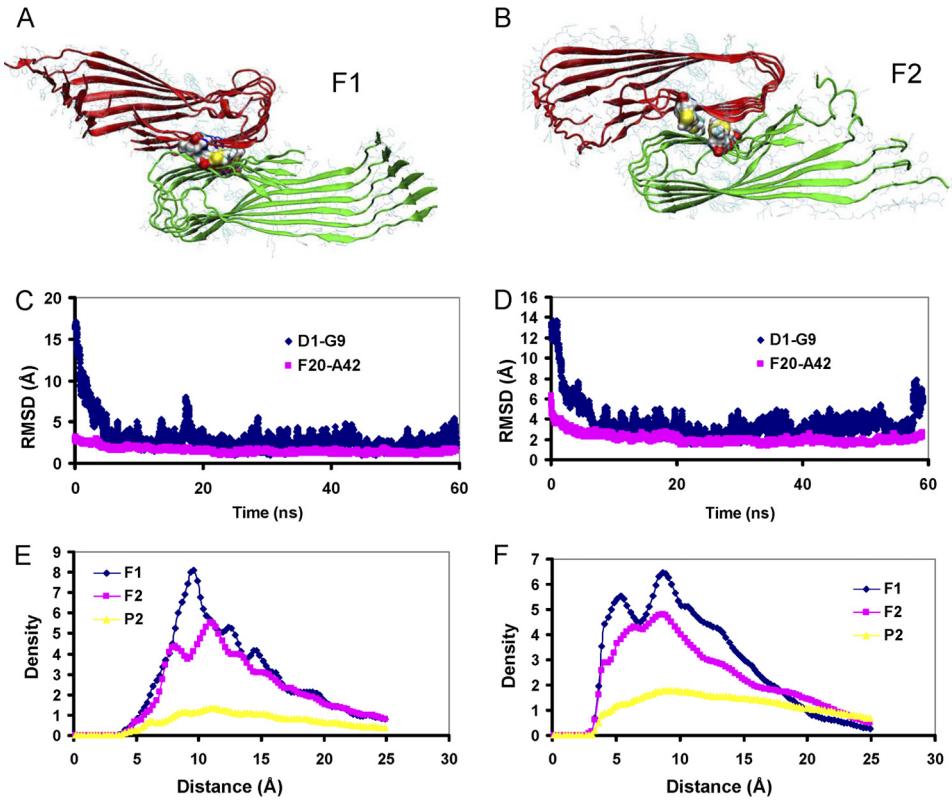

FIGURE 1. **The structure and dynamics of two Aβ fibril models (F1 and F2) indicate the importance of the Met-35 patch in fibril formation.** Each model consists of two hexamers organized in parallel that are packed together to yield a dodecamer. Each hexamer is a layer. The monomer has the well accepted U-shaped conformation. In the figure, the two U-shaped β-sheet layers are depicted in *red* and *green ribbons*. The Met-35 surface patches are highlighted (*yellow balls* are sulfur atoms, and *red balls* Met-35 are backbone oxygen). The coordinates are taken at the end of 60-ns simulations. *A*, the F1 model with turn structure based on the Luhrs structure (3). *B*, F2 model with turn structure based on Tycko's and our models (31, 33). *C* and *D*, the RMSD from averaged structures for both F1 (*C*) and F2 (*D*) show a flexible N-terminal and stable core structure. *E*, the distribution of the distances between the Cα atoms of the C-terminal residues 31–39 of two layers. *F*, the distribution of the distances between the heavy atoms of Met-35 with the heavy atoms in the C terminus of the next layer. The distance distributions for profibril oligomer P2 are also reported in *E* and *F* for comparison.

TABLE 1
Effective energy and relative population of Aβ42 dodecamers

Dodecamer models	Classification	Energy	Population if in equilibrium
		kcal/mol	*%*
F1	Fibril-like	−12095 ± 230	11.6
F2	Fibril-like	−12137 ± 237	12.2
FO1	Fibril oligomer	−12269 ± 236	13.8
FO2	Fibril oligomer	−11876 ± 274	8.5
P1	Prefibril oligomer	−11111 ± 192	1.3
P2	Prefibril oligomer	−11448 ± 216	3.6
P3	Preglobulomer oligomer	−11767 ± 201	6.8
P4	Preglobulomer oligomer	−11485 ± 220	3.9
GO1	Globulomer	−12264 ± 242	14.0
GO2	Globulomer	−12149 ± 242	12.4
GO3	Globulomer	−12106 ± 218	11.7

rithm. After 1 million steps, the conformations visited for each model were counted. The relative probability of model j was evaluated as follows,

$$P_j = N_j/N_{total} \quad \text{(Eq. 1)}$$

where P_j is the population, N_j is the total number of conformations visited for binding mode j, and N_{total} is the total number of steps.

RESULTS

Structure and Relative Energies of the Aβ42 Fibrillar Models—During the 60-ns simulations at 330 K, both fibril model structures F1 and F2 exhibit excellent stability in the core region, with the N-terminal region having large flexibility (Fig. 1, *C* and *D*). The RMSD from the averaged structure for the core region (residues 20–42) is only 2 Å, whereas that of the N-terminal region (residues 1–9) fluctuates ~4 Å and occasionally reaches 8 Å. Overall, the hydrogen bonds between the β-strands are well preserved during the MD simulations, except that the edge strands have relatively large fluctuations. The distances between two C-terminal regions (from two layers) are similar for F1 and F2, with the F1 model presenting slightly tighter associations (Fig. 1*E*). As can be seen in Fig. 1*E*, the distance distribution between the two C-terminal β-sheets for the F1 model peaks at 10 Å, indicating complementarity, whereas for the F2 model, the distance distribution is a little more diffuse. Nevertheless, the F2 model still has tight matches between the two C-terminal β-sheets. When the Aβ peptide forms a β-sheet with an in-register parallel arrangement, the Met-35 residues form a continuous patch in each β-sheet layer, as shown by the colored surface in Fig. 1 (both *A* and *B*). In the F1 model, the patches of Met-35 from one layer form the closest contact with the Met-35 patch on another layer, with a distance peak of 5–6 Å (Fig. 1*A*). In the F2 model, the distances between the two Met-35 patches are larger (Figs. 1*B*). In both models, the Met-35 patches are in close contact with the C terminus of another layer (Fig. 1*F*). Consistent with our previous observation of equal populations of the two turns in the p3 amyloid (34), our current calculations also show that both conformers have close effective potential energy (Table 1).

Comparing the NH solvation factors with experimental D/H exchange protection ratios (40–42) provided insight into amyloid structural features. Qualitatively, our results are mostly consistent with a fibrillar Aβ42 state, with limited solvent exposure of the Tyr-10 to Phe-20 and Ile-31 to Ala-42 regions (Fig. 2*A*). Quantitatively, both F1 and F2 models failed to correlate with the Aβ42 D/H exchange protection factors (supplemental Fig. S1). Instead, we observed that the F2 model correlates with structural features of Aβ40 ($r = 0.71$; supplemental Fig. S1*D*), which was prepared under conditions similar to those of Aβ42 (41). We then calculated the NH solvation factors for Aβ40 and

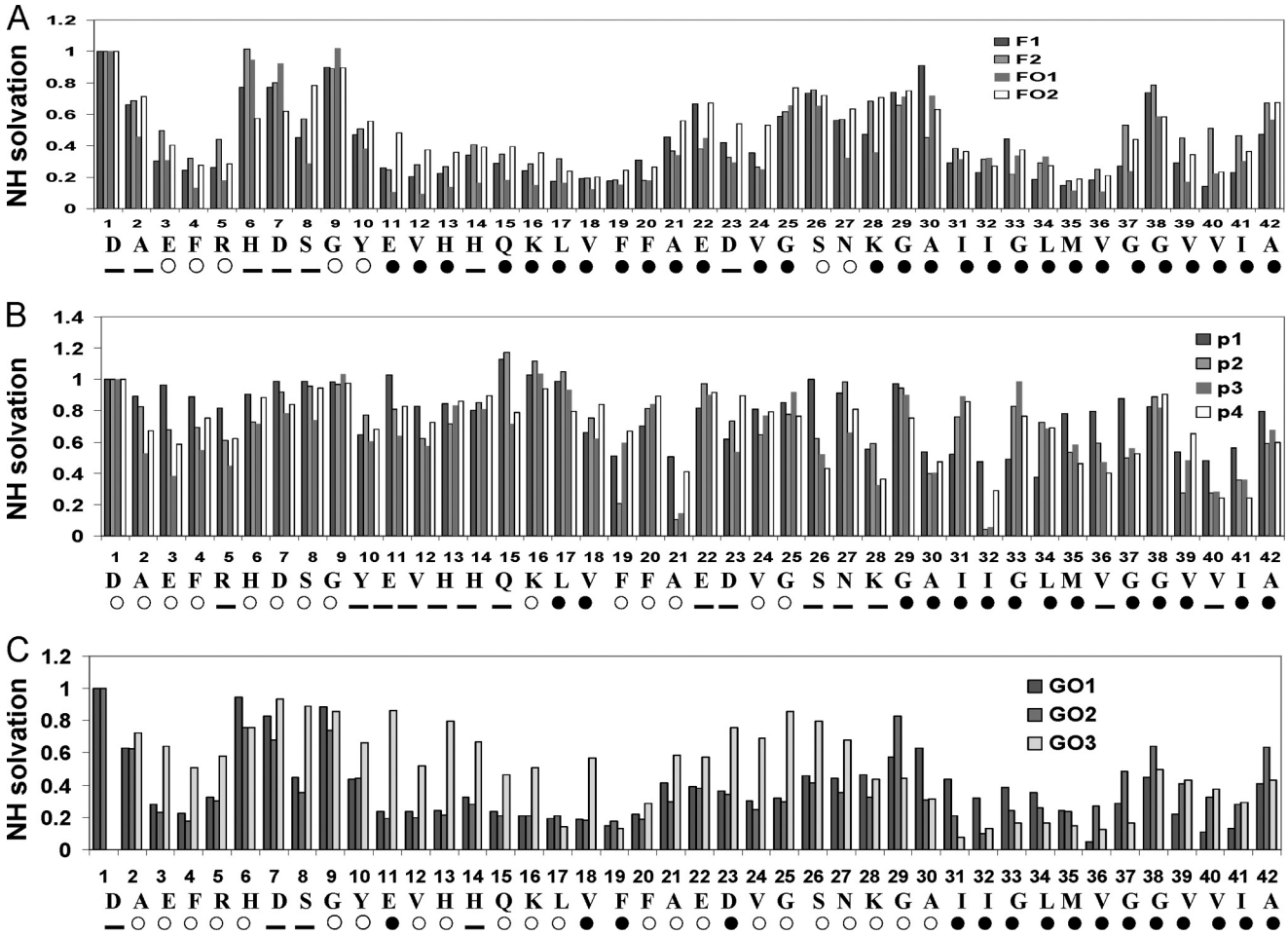

FIGURE 2. **Comparison of simulations with experiment: the simulated amide hydrogen protection factor (NH solvation on the *y* axis) *versus* the experimental H/D exchange NMR observations (*x* axis).** On the *x* axis, the residue number and type are listed, and the H/D exchange NMR factors are also indicated following reference (30). The *black circles* indicate highly protected residues, and the *white dots* show the decreasing protection; the *dashes* indicate no protection. *A*, fibril (F1 and F2) and fibril oligomer (FO1 and FO2) models. *B*, prefibril (P1 and P2) and preglobulomer (P3 and P4) models. *C*, globulomer models.

compared with those of F2 and confirmed that they are correlated with the experimental D/H exchange protection ratio (supplemental Table S1).

Electron cryo-microscopy suggested that Aβ40 and Aβ42 may have similar protofilament structures (43). However, the amide solvent protection analysis demonstrated that Aβ40 and Aβ42 may form different fibrillar structures under identical conditions (41). Apparently, polymorphic structural variations not included in our simulated fibril model lead to the low quantitative correlation of computed NH solvation factors with experimental D/H exchange protection ratios for Aβ42. An alternative conformation highlighted by Olofsson *et al.* (40), initially proposed by Petkova *et al.* (35), may represent a populated polymorphic form of Aβ; however, it does not correlate with the reported D/H exchange protection ratios for Aβ42. A possible explanation is that the Aβ42 fibril used for experimental D/H exchange protection measurement is a polymorphic assembly of fibrillar and globulomer organizations (see "Search for Possible Structures of the A-β Globulomer").

The Axial Growth of Aβ42 Fibrillar Oligomers Is Limited—If the FO is a one-layer unit of the Aβ42 fibril (28), it is expected that the FO could have behavior similar to that of the double-layer fibril structure. We simulated two FO models (FO1 and FO2; Figs. 3 and 4). However, both simulations showed that the Aβ42 FO does not retain an "ideal" half-unit structure as in the Aβ42 fibril. Extensive conformational changes occurred in both simulations. We observed two characteristics of the conformational dynamics of a single-layer fibrillar oligomer: the highly hydrophobic C terminus tends to "wrap" to minimize the exposed hydrophobic surface, and there is a fracture in the middle of the fibrillar oligomer (Figs. 3 and 4). In the fibril model, the highly hydrophobic C-terminal residues are buried. However, in the FO, these regions are exposed. Therefore, the FO tends to minimize exposure of hydrophobic surface area by bending in Gly-37 and Gly-38 (Figs. 3 and 4*C*), leading to C-terminal deviation from a planar β-sheet conformation. As can be seen in Fig. 3, part of the Met-35 patch is buried by Val-39, Val-40, Ile-41, and Ala-42. The bending is uneven for the U-shaped β-sheet strands with the edge strands presenting larger bending. This uneven bending to cover the exposed C-terminal hydrophobic surface causes stress in the single-layered FO structure. As a result, the β-sheet breaks up in the middle of the oligomer. In the FO1 simulation, the break

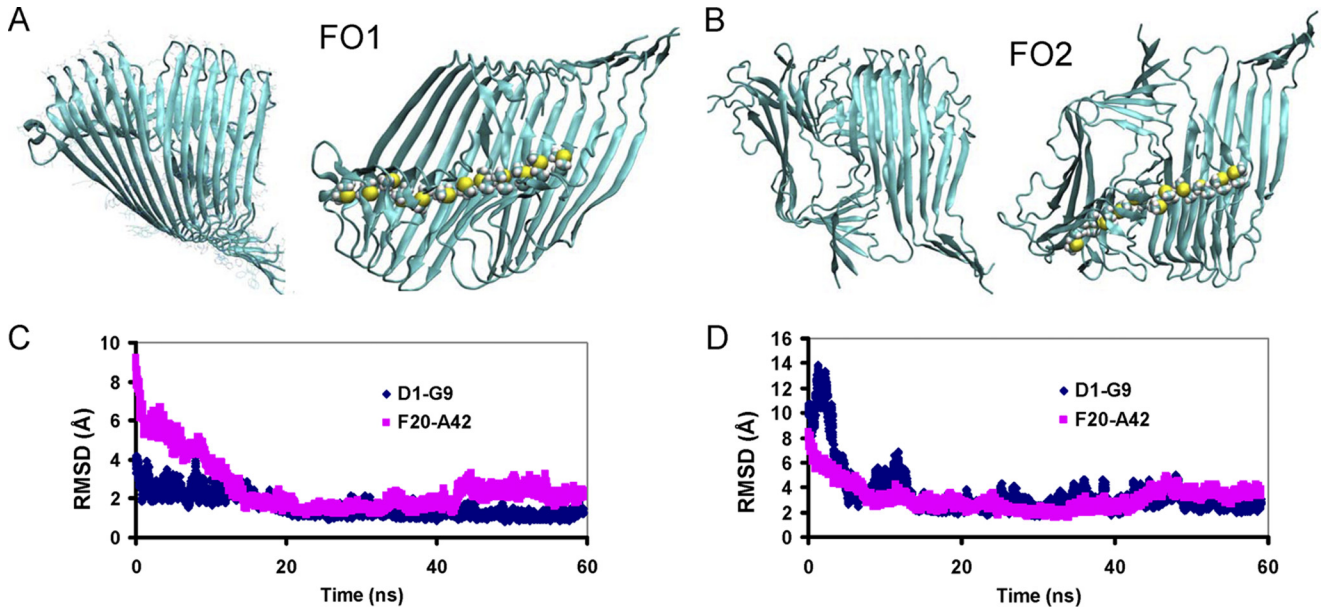

FIGURE 3. **Single layer fibril oligomer models have different structure and dynamics as compared with fibril models.** The fracture and C-terminal distortions are in the middle of the β-strands. *A*, FO1 model. The panel on the *left* provides a view from residues 10–24, showing the even fracture. On the *right* is the view from the C-terminal (residues 20–42) side, showing that Met-35 patch is partially covered. The *yellow balls* are sulfur atoms. *B*, FO2 model. On the *left* is the view from the side of residues 10–24, showing the large uneven fracture. On the *right* is the view from C-terminal (residues 20–42) side, showing that the Met-35 patch is partially covered. *C*, RMSD for the FO1 model. *D*, RMSD for the FO2 model.

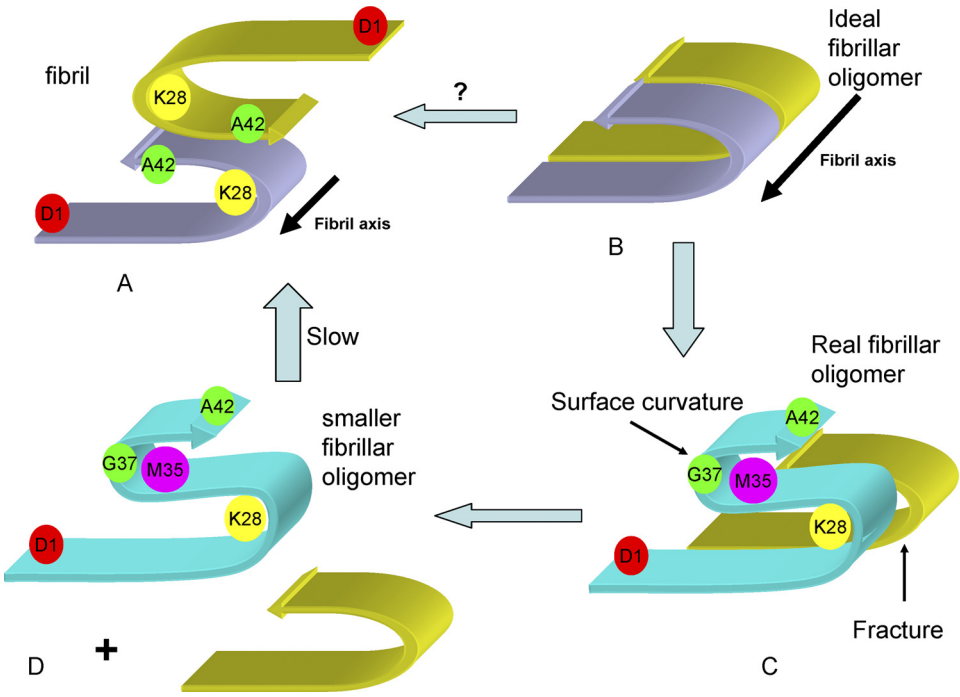

FIGURE 4. **This figure summarizes the essence of the paper from the mechanistic standpoint: the C-terminal distortions and β-sheet fracture explain why a fibril oligomer cannot directly convert to fibril.** *A* shows the fibril model represented by two U-shaped β-sheets associated via the C-terminal regions. Ideally, the fibril can be formed through binding of two ideal U-shaped β-sheets as represented in *B*. However, experiments indicate that *B* to *A* conversion is not straightforward. In our simulations, we found that the ideal "fibril" oligomer (*B*) is not stable in solution. Instead, the ideal fibril oligomer is better represented as the "real" fibril oligomer shown in *C*, with a fracture in the middle of the oligomer and nonplanar C terminus, in which Met-35 patch is covered. The longer structure of *C* would break into short pieces as indicated in *D*, which in turn either recruit more monomers or slowly convert to fibril in *A*. It is difficult to convert a longer fibril oligomer as in *C* to *A* because of the distortion of the C terminus.

occurs between strands six and seven (even break; Fig. 3*A*). In the FO2 simulation, strands five and six partially separate (uneven break; Fig. 3*B*).

These conformational changes reveal the mechanisms of (i) Aβ FO fracture and (ii) the barrier to directly convert the oligomer to Aβ fibril by simple "dimerization" of the half-unit. In the experiments of Wu *et al.* (28), the incubation of FOs does not lead to increasing length. Rather, FO incubation tends to yield an increase in the number of pieces, indicating that longer FOs break into shorter fragments. It is clear from our simulation that when the growth of the FO reaches a certain length, the stress build-up in the single layer β-sheet will break it into two pieces. Even though each fragmented piece can recruit more monomers leading to extension, they do not easily dimerize, mainly because the Met-35 patch is partially buried. Thus only a few populated FOs with extended C termini can associate and form fibrils. Such a mechanism is consistent with a recent model for conversion of Aβ42 neurotoxic oligomers into fibrils, which suggests that bending in the Gly-37 and Gly-38 region also occurs in small oligomers (44).

The energies of the FO models fluctuate significantly. Although the more ordered form (FO1) is more stable than the double-layered fibril form, the less ordered model (FO2) is much higher in

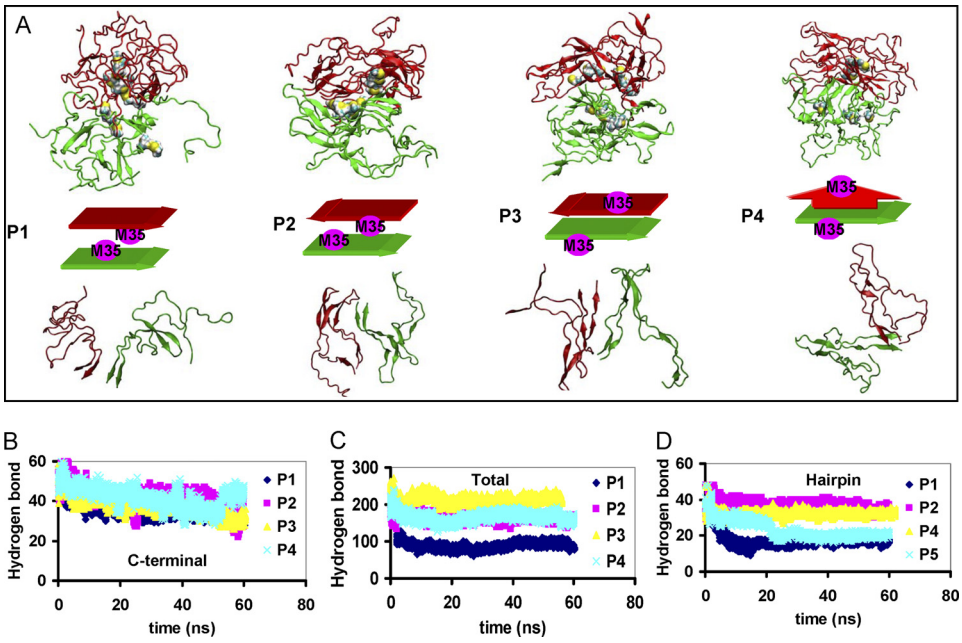

FIGURE 5. **The arrangement and secondary structure stabilities of prefibril oligomers (P1 and P2) and preglobulomer (P3 and P4).** *A*, the differences in Met-35 patch interactions. In each model, the Met-35 patches are shown in a surface representation with the *yellow balls* representing sulfur atoms. In the *top row*, six β-strands are represented as *red ribbons*, and another six as *green ribbons*, for comparison with Fig. 1. In the *middle*, there are two ways of arranging the C-terminal Met-35 patches as illustrated by block arrows. In models P1 and P2, the Met-35 patches are available to be associated as in fibril (Fig. 1). However, in P3 and P4 the Met-35 patches are not available, because they are covered by residues 1–20. In P3 and P4, the C terminus can be associated without Met-35 patches. The orientation of the C-terminal β-sheets can be parallel (P1), antiparallel (P2 and P3), or with an angle up to 90 degree (orthogonally, P4). In the *bottom row*, only four core strands are shown for clarity. *B*, the backbone hydrogen bond in C-terminal region along the simulation trajectories for the four models. *C*, the total number of backbone hydrogen bond. *D*, the number of hydrogen bonds in the hairpin region of residues Val-18 to Ile-32.

energy than the double-layered fibril models F1 and F2 (Table 1). Interestingly, the dynamics of the N and C termini are coupled. In the fibril models, the C-terminal region is completely buried between two layers, whereas the N terminus is more flexible. However, in the one-layer FO model where there is no C-terminal interaction between the two layers, the N terminus is relatively stable with small RMSD (Fig. 3, *C* and *D*).

The Prefibril Oligomer and Preglobulomer May Have Different C Termini Interactions with Respect to the Met-35 Patch—Yu *et al.* (30) have characterized the partially structured oligomers before they are converted to globulomers. Compared with the FO, these preglobulomers have similar C-terminal associations but differ in the 17–32 region. Because these species are expected to be very flexible and do not have well defined structure, it is difficult to construct a representative model. One would expect that there are a large number of possible arrangements for the prefibril or preglobulomer oligomers. The structural information of the preglobulomer reported by Yu *et al.* is the only one available experimentally. It is conceivable that (at least some of) the structural features observed in the preglobulomer could be shared by prefibrillar oligomers, at least in the parallel β-sheet C-terminal region.

We build four dodecamer models using the constraints of the experimentally observed β-sheet and β-hairpin patterns, mainly to compare these prefibril oligomer or preglobulomers with other fibril or globulomer models. We hypothesize that the major difference between the prefibril oligomers and the preglobulomers could be the ways that C termini from two layers associate. In the prefibril oligomer, the C terminus may either have Met-35 patches exposed or already associated in a similar way to that of the double-layered fibril. For the preglobulomer oligomers, the Met-35 patches are not available for fibril-like interactions. Thus we tested two major ways by which the C termini can associate: the first resembles that in the fibrillar structure with the Met from different layers associated (P1 and P2 in Fig. 5); the second resembles that in the fibrillar structure with Met-35 wrapped into intrasheet interactions with residues 1–32 and not involved in the interlayer association (P3 and P4; Fig. 5). Conceptually, the P2 pattern may easily allow the conversion to a fibrillar structure, whereas P3 and P4 have to go through more substantial rearrangements. The C-terminal β-sheet stabilities for all four models are similar (with similar counts of hydrogen bonds in the C termini; Fig. 5*B*). However, the distance distribution between the C termini for the prefibril oligomer is broader than for the fibril (Fig. 1, *E* and *F*). The preglobulomer oligomers (P3 and P4) have higher total hydrogen bond counts. Both the prefibril oligomer model P2 and preglobulomer model P3 could have stable antiparallel intrapeptide β-hairpins (Fig. 5*D*). The energetic stabilities of the four models follow the order of the hydrogen bond counts (Fig. 5*C*), with P3 showing the lowest energy among the four tested models (Table 1).

To compare with H/D exchange NMR spectroscopy experiments, we calculated the solvent exposure ratio of backbone amide hydrogens (Fig. 2*B*). The P3 model shows good agreement in the region near Phe-4 and the C terminus (residues 30–42) but not around the intrapeptide β-hairpins (residue 20–30). It seems that these intrapeptide β-hairpins are not isolated in experimentally observed preglobulomers, suggesting higher solvation protection. Model P3 still has stable peptide β-hairpins with larger solvent exposure, because these β-hairpins are mostly isolated. Thus the experimentally observed preglobulomers may resemble P3, but they are more compact than the P3 model around the intrapeptide β-hairpin region.

Search for Possible Structures of the Aβ Globulomer—Based on the hypothesis that the globulomer may derive from preglobulomer while retaining strong C-terminal interactions, we seek experimental observations to probe a possible stable globulomer structure with highly ordered β-strand interactions and well defined sizes. We focused on three possible clues: (i) although it is well established that lipid bilayers catalyze parallel and anti-parallel fibrillar formations, the observation that

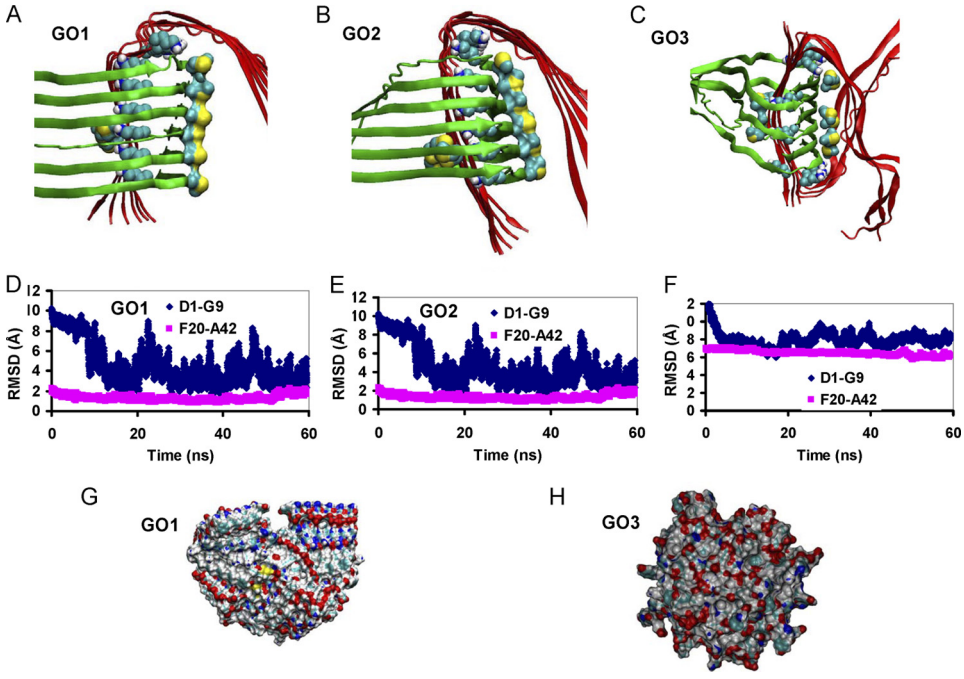

FIGURE 6. **The structure and dynamics of the globulomer models.** The two sets of six β-strands are represented as *red* and *green ribbons*. Lys-28 residues sit in the turn regions and are represented as *balls*. Met-35 patches are represented by surface patches, with sulfur atoms in *yellow*. *A*, the starting conformation for GO1 model, showing that with the Luhrs turn, two sets of six β-strands can fit exactly into an orthogonal C-terminal interaction, forming a dodecamer. *B*, the starting conformation for the GO2 model, showing that alternatively, two sets of six β-strands can also form an orthogonal C-terminal interaction with room for an additional strand in each set to form oligomer with 14 β-strands. *C*, starting conformation for the GO3 model with two sets of anti-parallel β-sheets (each with six strands), which also can form orthogonal C-terminal interactions. *D–F*, RMSDs of all three models exhibit large fluctuations of the N-terminal and stable core structures. *G* and *H*, surface model of residues 10–42 in the globulomer model, under the assumption that the flexible 1–9 region is not observable in EM.

fatty acids also induce globulomer formation (23) raises the possibility that globulomers could have some resemblance to lipid-binding proteins, and it is possible that globulomers have orthogonal β-sheets, similar to a dominant structural motif in lipid-binding proteins; this is consistent with the possible orthogonal β-sheets in the P4 model above. (ii) Lys-28 is highly protected in globulomers (23), which is similar to Lys-28 in the U-shaped β-sheets that have the Asp-23 to Lys-28 salt bridge buried in the turn; it seems reasonable to assume that matured globulomers could share the U-turn shape observed in fibril structures. (iii) Finally, globulomer sizes appear to favor 12 monomers, with some reaching 14 (23). The structural models illustrated in Fig. 6 (*A* and *B*) satisfy these experimental observations. The U-turn region is plastic (34), and at least two major turn forms were observed experimentally (3, 31). In model GO1, we retained the experimental turn structure from Lys-28 to Ala-42. This turn (the "Luhrs turn" (3)) structure can allow a maximum of 12 β-strands (two sets of six strands) to interact orthogonally (Fig. 6*A*). In the second model GO2 (Fig. 6*B*), the region of Lys-28 to Ala-42 is fully extended, corresponding to our turn structure (45) experimentally observed by the Tycko lab (35). The GO2 model, with a slightly longer Lys-28 to Ala-42 stretch, would allow up to 14 β-strands (two sets of seven strands) to interact orthogonally. Here we still use a dodecamer for the GO2 model, comparable with other structures. The third model GO3 (Fig. 6*C* and supplemental Fig. S2) was constructed with all of the β-strands in anti-parallel associations. Even though this model is not consistent with the suggestion of parallel β-sheet in spherical oligomers, it represents possible anti-parallel interactions. We note, however, that it is conceivable that other polymorphic conformational variants with different organizations could allow different sizes.

After 60 ns of MD simulations at 330 K, the C-terminal orthogonal β-sheets hold very well. The Met-35 patch in the GO1 model aligns near the edge of the β-sheet (residues 10–22; supplemental Fig. S2*A*). In the GO2 model, the Met-35 patch is covered by β-sheet residues 10–22 (supplemental Fig. S2*B*). For the GO3 model, the Met-35 patch is covered because of anti-parallel β-strand constraints (supplemental Fig. S2*C*). For the GO1 and GO2 models, even though residues 1–9 are still associated in a β-sheet, they fly around together, presenting very large RMSDs compared with the average structure, whereas residues 20–42 are stable (Fig. 6, *D* and *E*). Residues Asp-1 to His-14 are completely random in the model GO3.

If we assume that the highly flexible residues 1–9 cannot be observed by EM, the remaining parts of all three models could have round shapes like the globulomer "spherical" particles (Fig. 6, *G* and *H*). Among the three models, GO1 has the best average energy (Table 1), whereas GO3 has the highest energy. The energetic stability of GO1 is very close to that of FO2, indicating that both oligomers could have similar populations and that their formation is controlled by kinetics.

Surprisingly, we found that the computed NH solvation factors for the GO3 model correlate with the experimental D/H exchange protection ratios for Aβ42 ($r = 0.73$; supplemental Fig. S1*E*). The correlation with Aβ40 is much lower, and there is no correlation between the GO1 and GO2 models with the Aβ40 and Aβ42 fibrils. There are several possible explanations. It is possible that the Aβ42 fibril used in the experimental D/H exchange protection measurement is an ensemble of fibrillar and Aβ42 globulomers. Alternatively, Aβ42 fibril may have structural features similar to those of the GO3 globular model. The correlation indicates that our globulomer model with orthogonal β-sheets could exist.

DISCUSSION

How the Aβ peptides assemble and form toxic entities and what is the mechanism of toxicity are major questions in Alzheimer research. To address such questions, it is essential to have working structural models of small Aβ oligomers. Structural features of Aβ have been increasingly revealed by solution

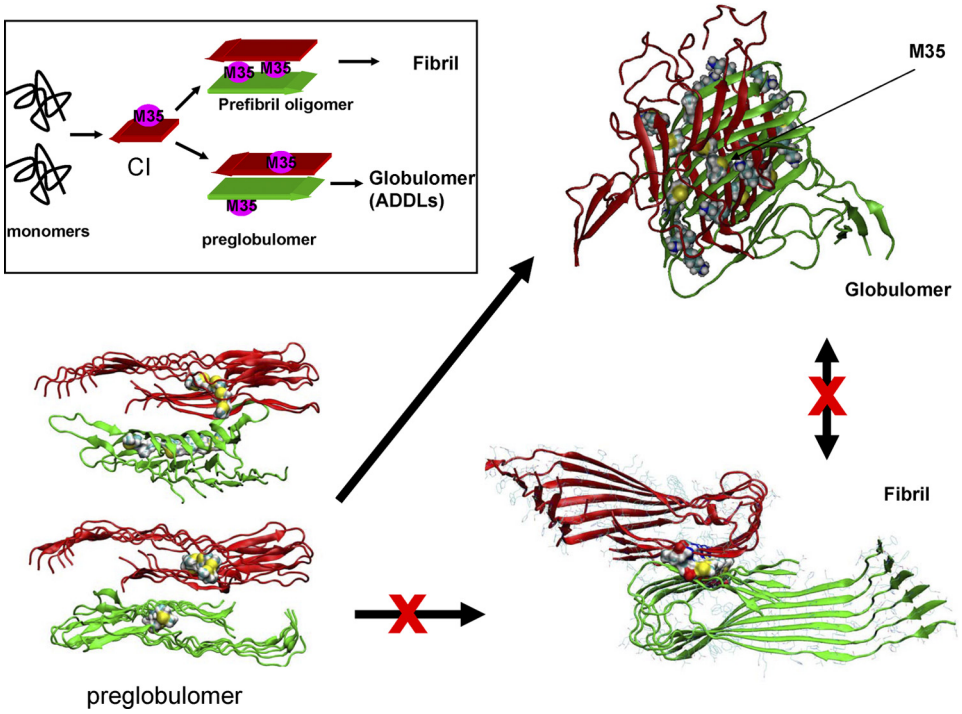

FIGURE 7. **The box illustrates that the fibril- and ADDL-forming pathways may share common critical intermediates and subsequently diverge into different structures.** The key step may involve the formation of critical intermediate (*CI*) with a C-terminal parallel β-sheet. The subsequent association of the critical intermediate may underlie the divergence of fibril and ADDL pathways. If the critical intermediate associates, leaving the Met-35 patches available, the fibril may eventually form. If the critical intermediates interact otherwise with Met-35 patches covered by other parts, ADDLs may be formed. The ribbon models (with six strands in *red* and six strands in *green*) highlight that critical intermediate interaction without Met-15 patches can mature into globulomer with orthogonal C-terminal interaction, with no conversion to fibril.

NMR (3, 30), solid state NMR (31, 46, 47), cryo-EM (48), and biochemical studies (23), leading to increased understanding of polymorphic Aβ fibrillar states in small Aβ oligomers. Among these small Aβ oligomers, double-layered and single-layered fibril oligomer structural models may provide pivotal insights, allowing further probing of elusive nonfibril oligomers. Our simulations of solvation protection of F1 and F2 models have reproduced experimental observations of Aβ fibrils (30) in several respects, including the observation that the three residues around F4 are structured. This observation is also consistent with another study that shows the higher stability of F4 in the Aβ amyloid (40, 41). Our dodecamer models of the Aβ fibril present higher flexibility of residues Gly-37 and Gly-38, which is also reflected by H/D exchange experiments (42).

The Aβ globulomer models (GO1 and GO2) satisfy experimental observations, and the simulated solvation protection factors for GO1 present good agreement with the experiment (30). Our simulations also indicate that the GO1 model could be the most stable species for Aβ dodecamers. The correlation of the NH solvation factors of the GO3 model with experimental D/H exchange protection ratio for the Aβ42 fibril may suggest that the globular model studied here has a biological role.

The major difference between the structures of the Aβ fibril and the globulomer centers on how the C termini of two β-sheet layers interact. Our results suggest that in the globulomer they pack together orthogonally, whereas in the fibril their interaction is antiparallel. Although the Met-35 patches in the Aβ fibril form highly complementary interactions between the two layers, in the globulomer they are buried intrasheet. These differences make it difficult for the globulomer to extend into a fibril (Fig. 7). The exposure of the Met-35 patch may be a key structural difference between the fibril- or ADDL-forming pathways.

What are the missing links between the ADDL and protofibrils (49)? Our proposed mechanism for the formation of the fibril and globulomer points to the β-sheet of the highly hydrophobic C-terminal region, consistent with the NMR study of the preglobulomer (30). As illustrated in the box of Fig. 7, after the formation of the C-terminal β-sheet, there are two ways for it to interact: the first is by using the Met-35 patch surface, which leads to fibril formation, and the second is using the surface without the Met-35 patch, which would favor globulomer formation. Because the formation of a C-terminal β-sheet is critical in both pathways, it may constitute a "critical intermediate." We further note that because the ensemble of oligomers reflect population shifts on a rugged energy landscape (16, 17), a change in the environment can easily shift the population toward a specific pathway and outcome.

The broad Aβ oligomer variability presents a problem in AD drug design and in planning other therapeutic approaches. Targeting toxicity in an AD late stage may miss the reservoir of polymorphic forms. If common links among polymorphic states can be established, then targeting the bottleneck would be more effective. Among these, critical intermediates could be such AD targets.

Targeting the Met-35 patch to inhibit Aβ42 and Aβ42 toxicity has already been attempted (50). Met-35 oxidation frequently occurs *in vivo* and has been suggested to be involved in Aβ-induced oxidative damage (51). Based on our current study, we propose that Met-35 oxidation might decrease both ADDL and fibril formation caused by increased polarity of oxidized Met-35. Oxidized Met-35 will increase the tendency to be exposed to water and decrease the propensity of ADDL formation. However, because of the polymorphic nature of the Aβ protofibril, fibril formation may be less affected. Consistently, it has been found that Met-35 oxidation decreases paranucleus formation (21) and reduces Aβ42 toxicity (52).

In a transgenic AD mouse model (with an M631L mutation) where Met-35 was mutated to Leu, oxidative stress damage would be prevented, and Aβ-immunoreative plaques can be expected to be reduced. Instead, small punctuated immunoreactive nonplaque areas were still found (53). This could relate to

increased ADDL population, which favors lower exposure of hydrophobic Leu.

Mutations near the Met region also impede fibril formation, like G33L and G37L (50) and G33V and G37D (54, 55). Kim and Hecht (56) systematically studied 20 mutants at 17 positions in Aβ42. It would also be interesting to switch the Gly-33 and Met-35 or Met-35 and Gly-37. Although we may expect that the dimer interface would be less affected than the ADDL, the pathway population may also change.

Acknowledgment—We thank Professor Normand Mousseau for discussions.

REFERENCES

1. Ahmad, A., Millett, I. S., Doniach, S., Uversky, V. N., and Fink, A. L. (2004) *J. Biol. Chem.* **279,** 14999–15013
2. Pitschke, M., Prior, R., Haupt, M., and Riesner, D. (1998) *Nat. Med.* **4,** 832–834
3. Lührs, T., Ritter, C., Adrian, M., Riek-Loher, D., Bohrmann, B., Döbeli, H., Schubert, D., and Riek, R. (2005) *Proc. Natl. Acad. Sci. U.S.A.* **102,** 17342–17347
4. Kirkitadze, M. D., Bitan, G., and Teplow, D. B. (2002) *J. Neurosci. Res.* **69,** 567–577
5. Walsh, D. M., and Selkoe, D. J. (2004) *Protein Pept. Lett.* **11,** 213–228
6. Hardy, J., and Selkoe, D. J. (2002) *Science* **297,** 353–356
7. Kayed, R., Head, E., Thompson, J. L., McIntire, T. M., Milton, S. C., Cotman, C. W., and Glabe, C. G. (2003) *Science* **300,** 486–489
8. Baumketner, A., Bernstein, S. L., Wyttenbach, T., Bitan, G., Teplow, D. B., Bowers, M. T., and Shea, J. E. (2006) *Protein Sci.* **15,** 420–428
9. Jang, H., Zheng, J., and Nussinov, R. (2007) *Biophys. J.* **93,** 1938–1949
10. Jang, H., Zheng, J., Lal, R., and Nussinov, R. (2008) *Trends Biochem. Sci.* **33,** 91–100
11. Masuda, Y., Uemura, S., Ohashi, R., Nakanishi, A., Takegoshi, K., Shimizu, T., Shirasawa, T., and Irie, K. (2009) *ChemBioChem* **10,** 287–295
12. Jang, H., Ma, B., Lal, R., and Nussinov, R. (2008) *Biophys. J.* **95,** 4631–4642
13. Mustata, M., Capone, R., Jang, H., Arce, F. T., Ramachandran, S., Lal, R., and Nussinov, R. (2009) *J. Am. Chem. Soc.* **131,** 14938–14945
14. Kusumoto, Y., Lomakin, A., Teplow, D. B., and Benedek, G. B. (1998) *Proc. Natl. Acad. Sci. U.S.A.* **95,** 12277–12282
15. Petkova, A. T., Buntkowsky, G., Dyda, F., Leapman, R. D., Yau, W. M., and Tycko, R. (2004) *J. Mol. Biol.* **335,** 247–260
16. Miller, Y., Ma, B., and Nussinov, R. (2010) *Proc. Natl. Acad. Sci. U.S.A.* **107,** 14128–14133
17. Miller, Y., Ma, B., and Nussinov, R. (2010) *Chem. Rev.* **110,** 4820–4838
18. Ma, B., Kumar, S., Tsai, C. J., and Nussinov, R. (1999) *Protein Eng.* **12,** 713–720
19. Tsai, C. J., Ma, B., and Nussinov, R. (1999) *Proc. Natl. Acad. Sci. U.S.A.* **96,** 9970–9972
20. Arispe, N., Pollard, H. B., and Rojas, E. (1994) *Mol. Cell Biochem.* **140,** 119–125
21. Bitan, G., Tarus, B., Vollers, S. S., Lashuel, H. A., Condron, M. M., Straub, J. E., and Teplow, D. B. (2003) *J. Am. Chem. Soc.* **125,** 15359–15365
22. Lambert, M. P., Barlow, A. K., Chromy, B. A., Edwards, C., Freed, R., Liosatos, M., Morgan, T. E., Rozovsky, I., Trommer, B., Viola, K. L., Wals, P., Zhang, C., Finch, C. E., Krafft, G. A., and Klein, W. L. (1998) *Proc. Natl. Acad. Sci. U.S.A.* **95,** 6448–6453
23. Barghorn, S., Nimmrich, V., Striebinger, A., Krantz, C., Keller, P., Janson, B., Bahr, M., Schmidt, M., Bitner, R. S., Harlan, J., Barlow, E., Ebert, U., and Hillen, H. (2005) *J. Neurochem.* **95,** 834–847
24. Gellermann, G. P., Byrnes, H., Striebinger, A., Ullrich, K., Mueller, R., Hillen, H., and Barghorn, S. (2008) *Neurobiol. Dis.* **30,** 212–220
25. Lesné, S., Koh, M. T., Kotilinek, L., Kayed, R., Glabe, C. G., Yang, A., Gallagher, M., and Ashe, K. H. (2006) *Nature* **440,** 352–357
26. Hoshi, M., Sato, M., Matsumoto, S., Noguchi, A., Yasutake, K., Yoshida, N., and Sato, K. (2003) *Proc. Natl. Acad. Sci. U.S.A.* **100,** 6370–6375
27. Noguchi, A., Matsumura, S., Dezawa, M., Tada, M., Yanazawa, M., Ito, A., Akioka, M., Kikuchi, S., Sato, M., Ideno, S., Noda, M., Fukunari, A., Muramatsu, S., Itokazu, Y., Sato, K., Takahashi, H., Teplow, D. B., Nabeshima, Y., Kakita, A., Imahori, K., and Hoshi, M. (2009) *J. Biol. Chem.* **284,** 32895–32905
28. Wu, J. W., Breydo, L., Isas, J. M., Lee, J., Kuznetsov, Y. G., Langen, R., and Glabe, C. (2010) *J. Biol. Chem.* **285,** 6071–6079
29. Chimon, S., Shaibat, M. A., Jones, C. R., Calero, D. C., Aizezi, B., and Ishii, Y. (2007) *Nat. Struct. Mol. Biol.* **14,** 1157–1164
30. Yu, L., Edalji, R., Harlan, J. E., Holzman, T. F., Lopez, A. P., Labkovsky, B., Hillen, H., Barghorn, S., Ebert, U., Richardson, P. L., Miesbauer, L., Solomon, L., Bartley, D., Walter, K., Johnson, R. W., Hajduk, P. J., and Olejniczak, E. T. (2009) *Biochemistry* **48,** 1870–1877
31. Petkova, A. T., Yau, W. M., and Tycko, R. (2006) *Biochemistry* **45,** 498–512
32. Zheng, J., Jang, H., Ma, B., Tsai, C. J., and Nussinov, R. (2007) *Biophys. J.* **93,** 3046–3057
33. Ma, B., and Nussinov, R. (2002) *Proc. Natl. Acad. Sci. U.S.A.* **99,** 14126–14131
34. Miller, Y., Ma, B., and Nussinov, R. (2009) *Biophys. J.* **97,** 1168–1177
35. Petkova, A. T., Ishii, Y., Balbach, J. J., Antzutkin, O. N., Leapman, R. D., Delaglio, F., and Tycko, R. (2002) *Proc. Natl. Acad. Sci. U.S.A.* **99,** 16742–16747
36. Phillips, J. C., Braun, R., Wang, W., Gumbart, J., Tajkhorshid, E., Villa, E., Chipot, C., Skeel, R. D., Kalé, L., and Schulten, K. (2005) *J. Comput. Chem.* **26,** 1781–1802
37. MacKerell, A. D., Bashford, D., Bellott, M., Dunbrack, R. L., Evanseck, J. D., Field, M. J., Fischer, S., Gao, J., Guo, H., Ha, S., Joseph-McCarthy, D., Kuchnir, L., Kuczera, K., Lau, F. T., Mattos, C., Michnick, S., Ngo, T., Nguyen, D. T., Prodhom, B., Reiher, W. E., Roux, B., Schlenkrich, M., Smith, J. C., Stote, R., Straub, J., Watanabe, M., Wiorkiewicz-Kuczera, J., Yin, D., and Karplus, M. (1998) *J. Phys. Chem. B* **102,** 3586–3616
38. Darden, T., York, D., and Pedersen, L. (1993) *J. Chem. Phys.* **98,** 10089–10092
39. Lee, M. S., Salsbury, F. R., and Brooks, C. L. (2002) *J. Chem. Phys.* **116,** 10606–10614
40. Olofsson, A., Sauer-Eriksson, A. E., and Ohman, A. (2006) *J. Biol. Chem.* **281,** 477–483
41. Olofsson, A., Lindhagen-Persson, M., Sauer-Eriksson, A. E., and Ohman, A. (2007) *Biochem. J.* **404,** 63–70
42. Olofsson, A., Sauer-Eriksson, A. E., and Ohman, A. (2009) *Anal. Biochem.* **385,** 374–376
43. Schmidt, M., Sachse, C., Richter, W., Xu, C., Fändrich, M., and Grigorieff, N. (2009) *Proc. Natl. Acad. Sci. U.S.A.* **106,** 19813–19818
44. Ahmed, M., Davis, J., Aucoin, D., Sato, T., Ahuja, S., Aimoto, S., Elliott, J. I., Van Nostrand, W. E., and Smith, S. O. (2010) *Nat. Struct. Mol. Biol.* **17,** 561–567
45. Ma, B., and Nussinov, R. (2002) *Protein Sci.* **11,** 2335–2350
46. Petkova, A. T., Leapman, R. D., Guo, Z., Yau, W. M., Mattson, M. P., and Tycko, R. (2005) *Science* **307,** 262–265
47. Paravastu, A. K., Leapman, R. D., Yau, W. M., and Tycko, R. (2008) *Proc. Natl. Acad. Sci. U.S.A.* **105,** 18349–18354
48. Zhang, R., Hu, X., Khant, H., Ludtke, S. J., Chiu, W., Schmid, M. F., Frieden, C., and Lee, J. M. (2009) *Proc. Natl. Acad. Sci. U.S.A.* **106,** 4653–4658
49. Klein, W. L. (2002) *Neurobiol. Aging* **23,** 231–235
50. Sato, T., Kienlen-Campard, P., Ahmed, M., Liu, W., Li, H., Elliott, J. I., Aimoto, S., Constantinescu, S. N., Octave, J. N., and Smith, S. O. (2006) *Biochemistry* **45,** 5503–5516
51. Butterfield, D. A., and Kanski, J. (2002) *Peptides* **23,** 1299–1309
52. Misiti, F., Clementi, M. E., and Giardina, B. (2010) *Neurochem. Int.* **56,** 597–602
53. Butterfield, D. A., Galvan, V., Lange, M. B., Tang, H., Sowell, R. A., Spilman, P., Fombonne, J., Gorostiza, O., Zhang, J., Sultana, R., and Bredesen, D. E. (2010) *Free Radic. Biol. Med.* **48,** 136–144
54. Kanski, J., Varadarajan, S., Aksenova, M., and Butterfield, D. A. (2002) *Biochim. Biophys. Acta* **1586,** 190–198
55. Kanski, J., Aksenova, M., and Butterfield, D. A. (2002) *Neurotox. Res.* **4,** 219–223
56. Kim, W., and Hecht, M. H. (2008) *J. Mol. Biol.* **377,** 565–574